4

K-DISTRIBUTION AND POLARIMETRIC TERRAIN RADAR CLUTTER

S. H. Yueh, J. A. Kong, J. K. Jao, R. T. Shin
H. A. Zebker, T. Le Toan, and H. Ōttl

4.1 Introduction

Polarimetric terrain backscatter data observed with satellite and airborne synthetic aperture radars (SAR) have demonstrated potential applications in geologic mapping and terrain cover classification [1-8]. In previous publications on this subject, Gaussian statistics have been frequently assumed for the radar return signals to build the Bayes terrain classifier [1-3]. However, abundant experimental evidence shows

that terrain radar clutter is non-Gaussian, i.e., non-Rayleigh in amplitude distribution [9-12].

Among many non-Gaussian statistics, the K-distribution has proven to be useful in characterizing the amplitude distribution of electromagnetic echoes from various objects [10-18], including diverse ground surfaces [10], sea surface [11] and wave propagation through atmospheric turbulence [14,15,18]. To derive the K-distribution, a two-dimensional isotropic random walk model with a negative-binomial-distributed number of steps has been used [13] and extended to n-dimension space [14,17]. Furthermore, in the case of the weak scattering regime, the assumption of a nonuniform phase distribution for each vector step [15], or, alternatively, the assumption of a directional bias [17], has been shown to lead to a generalized K-distribution. Unfortunately, this approach is not directly applicable to polarimetric scattering data because of the correlation among polarizations and different variances of each polarization [19,20]. This difficulty may be circumvented by including properly the covariances of the polarizations in the multivariate K-distribution [21].

By assuming a product model where the received polarimetric returns are the product of a complex Gaussian random vector and a Gamma-distributed scaling factor, a K-distribution with two parameters, ν and $\overline{\sigma}$, was derived in [22]. In this chapter, another approach, a clustered terrain scatterer model [10], is used to derive the K-distribution with one parameter, α. By setting $\nu = \alpha$ and $\overline{\sigma} = 1/\alpha$, the result of [22] can be transformed into (11) in this chapter. After experimental data are analyzed, it is found that one parameter α is sufficient to characterize polarimetric terrain clutter [21].

In section 4.2, the n-dimensional anisotropic random walk model is used to generalize the approach of [13] to derive the zero-mean multivariate K-distribution for polarimetric data. Anisotropy refers to the fact that the polarimetric covariance matrix is not proportional to an identity matrix. The polarimetric amplitude data are normalized by the square root of the illuminated area so that the measured covariances of the polarimetric data are in terms of scattering cross section per unit area. The polarimetric covariance matrix is shown to be directly related to that of a single scatterer. The result is then generalized to the nonzero-mean multivariate K-distribution. There are two ways to introduce nonzero mean into the K-distribution. The directional bias random walk model will lead to a generalized K-distribution [17], and

the homodyned approach will result in a homodyned K-distribution [13,17]. We will apply both approaches in deriving the nonzero mean K-distribution and discuss the corresponding scattering processes. In order to apply the K-distribution to the normalized polarimetric classifier problem [2,3], the probability density function (PDF) of the normalized K-distributed vector is derived and discussed in section 4.3. In section 4.4, four sets of experimental data, obtained from MIT Lincoln Laboratory, the Jet Propulsion Laboratory (JPL), and the German Aerospace Research Establishment (DLR) of the Federal Republic of Germany, are compared with the K-distribution to lend support to the above model.

4.2 Multivariate K-distribution and Anisotropic Random Walk Model

It will be shown in this section that the polarimetric scattering data, HH, HV, VH, and VV, will be multivariately K-distributed if the number of scatterers within the region illuminated by the electromagnetic wave has a negative binomial distribution. The zero-mean K-distribution will be derived first. Subsequently, the nonzero-mean case will be addressed.

a. Zero-mean Multivariate K-distribution

By assuming that there are randomly distributed scatterers of a single type inside the illuminated region and neglecting the multiple scattering between scatterers, the received polarimetric data $\overline{X}_{rec}$ can be written as the sum of the polarimetric data from each of N scatterers. Since the polarimetric return from the terrain cover is generally zero mean [19,20], the received signal can be modeled as an N-step n-dimensional random walk with the resultant displacement given by

$$\overline{X}_{rec} = \sum_{j=1}^{N} \overline{X}_j \tag{1}$$

where $\overline{X}_j$ is the scattered polarimetric data from the jth scatterer and all $\overline{X}_j$ are independent identically distributed n-dimensional random vectors with zero mean, i.e., $E(\overline{X}_j) = 0$. The dimension of $\overline{X}_{rec}$ is taken to be eight, considering the I (in phase) and Q (quadrature phase) components of HH, HV, VH, and VV separately. For the polarimetric

backscattering from a reciprocal medium, where HV equals to VH, the dimension of $\overline{X}_{rec}$ is six.

For the case of terrain and sea returns, the cross section is normalized with respect to the area A illuminated by the radar. Thus the polarimetric data are given as

$$\overline{X} = \frac{1}{\sqrt{A}} \sum_{j=1}^{N} \overline{X}_j \tag{2}$$

Because all $\overline{X}_j$ are assumed to be independent, the characteristic function of $\overline{X}$, given the number of steps N, is

$$\Phi_N(\overline{k}) = \phi\left(\frac{\overline{k}}{\sqrt{A}}\right)^N \tag{3}$$

where $\phi(\overline{k})$ is the characteristic function of $\overline{X}_j$,

$$\phi(\overline{k}) = \int e^{i\overline{k}\cdot\overline{X}_j} P(\overline{X}_j) d\overline{X}_j \tag{4}$$

Now let N be a negative binomial random variable such that its probability function, specified by the average number of steps N_a and a parameter α, is

$$P(N) = \binom{N+\alpha-1}{N} \frac{(N_a/\alpha)^N}{(1+N_a/\alpha)^{N+\alpha}} \tag{5}$$

where N_a can be interpreted as the average number of scatterers observed within the illuminated region. Note that the negative binomial distribution is the steady state solution of the birth-death-immigration random process [10,13].

Then averaging (3) over N, we have the unconditioned characteristic function of $\overline{X}$,

$$\Phi_{N_a}(\overline{k}) = \left\{1 + \frac{N_a}{\alpha}\left[1 - \phi\left(\frac{\overline{k}}{\sqrt{A}}\right)\right]\right\}^{-\alpha} \tag{6}$$

As the illuminated area A approaches infinity, the characteristic function can be approximated by the Taylor series to second order

$$\phi\left(\frac{\overline{k}}{\sqrt{A}}\right) = 1 - \frac{1}{2A}\overline{k}^T \cdot \overline{\overline{C}}_s \cdot \overline{k} \tag{7}$$

where

$$\overline{\overline{C}}_s = E(\overline{X}_j \overline{X}_j^T) \tag{8}$$

represents the polarimetric scattering characteristics of each single scatterer. In general, $\overline{\overline{C}}_s$, which contains information regarding the geometry and the constituents of each single scatterer, is a function of the probing radar frequency and look angle and can be determined analytically by electromagnetic wave theory or by experimental measurement. For example, $\overline{\overline{C}}_s$ for leaves of vegetation will be influenced by the distribution of the shape, tilt angle, and permittivity of the leaves.

Substituting (7) into (6), we then have

$$\Phi_{N_a}(\overline{k}) = \left[1 + \frac{1}{2\alpha}\overline{k}^T \cdot \overline{\overline{C}} \cdot \overline{k}\right]^{-\alpha} \tag{9}$$

where

$$\overline{\overline{C}} = \frac{N_a \overline{\overline{C}}_s}{A} \tag{10}$$

is the fully polarimetric covariance matrix [20,21] measured by the radar system.

The characteristic function (9) is the generalization of the n-dimensional isotropic random walk model [14,17]; however, the correlations between different polarizations are now included and can be attributed to the fundamental scattering properties, $\overline{\overline{C}}_s$, of a single scatterer. The corresponding limiting distribution of $\overline{X}$ is obtained by the inverse Fourier transform in appendix A and becomes the multivariate K-distribution,

$$P(\overline{X}) = \frac{1}{(2\pi)^{n/2}|\overline{\overline{C}}|^{1/2}} \frac{(2\alpha)^{n/4+\alpha/2}(\overline{X}^T \cdot \overline{\overline{C}}^{-1} \cdot \overline{X})^{\alpha/2-n/4}}{2^{\alpha-1}\Gamma(\alpha)} \times K_{n/2-\alpha}\left[\sqrt{2\alpha}(\overline{X}^T \cdot \overline{\overline{C}}^{-1} \cdot \overline{X})^{1/2}\right] \tag{11}$$

The multivariate K-distribution reduces to that of an isotropic model [14,17], when the covariance matrix is a diagonal matrix with equal variances. As the parameter α goes to infinity, (9) and (11) approach the characteristic function and probability density function, respectively, of the Gaussian distribution. An alternative derivation of the multivariate K-distribution is given in appendix B.

If the I and Q components of the returns at each polarization are of equal variance and uncorrelated, the amplitude distribution for the return at each polarization reduces to that of the two-dimensional isotropic random walk case [10,13] and is given as

$$p(x) = \frac{4\alpha^{1/2+\alpha/2}}{\Gamma(\alpha)} x^{\alpha} K_{\alpha-1}(2\alpha^{1/2}x) \tag{12}$$

where the variable x is

$$x = \frac{|HH|}{\sqrt{<|HH|^2>}}, \text{ or } \frac{|HV|}{\sqrt{<|HV|^2>}}, \text{ or } \frac{|VV|}{\sqrt{<|VV|^2>}}. \tag{13}$$

The normalized intensity moments of HH, HV, and VV are defined as follows,

$$I_{HH}^{(m)} = \frac{<|HH|^{2m}>}{<|HH|^2>^m} \tag{14a}$$

$$I_{HV}^{(m)} = \frac{<|HV|^{2m}>}{<|HV|^2>^m} \tag{14b}$$

$$I_{VV}^{(m)} = \frac{<|VV|^{2m}>}{<|VV|^2>^m} \tag{14c}$$

where the superscript m denotes the order of normalized intensity moments. The normalized intensity moments of the K-distributed zero-mean feature vector are given as [13]

$$I^{(m)} = \frac{m!\Gamma(m+\alpha)}{\alpha^m \Gamma(\alpha)} \tag{15}$$

which can be obtained by using (C1) in appendix C.

In particular, the second-order normalized intensity moment is given as

$$I^{(2)} = 2\left(1 + \frac{1}{\alpha}\right) \tag{16}$$

For a zero-mean Gaussian random vector, α is infinity and $I^{(2)}$ equals 2. Equation (16) will be used in section 4.4 to estimate the parameter α which best matches experimental data sets.

b. Nonzero-mean Multivariate K-distribution

In order to model the radar return from a target in the presence of K-distributed clutter or the wave propagation through atmospheric turbulence (radio-link communications) [15,18], the nonzero-mean case is considered next. There are two ways to model the nonzero mean case. The first is the homodyned approach [13] where the received unnormalized field is viewed as two terms superimposed, the mean field $\overline{\mu}_t$ and the fluctuation field $\overline{X}_f$,

$$\overline{X}_{rec} = \overline{\mu}_t + \overline{X}_f \tag{17a}$$

$$\overline{X}_f = \sum_{j=1}^{N} \overline{X}_j \tag{17b}$$

The mean field $\overline{\mu}_t$ can be interpreted in the following ways. For radio-link communications, $\overline{\mu}_t$ is the transmitted radio signal which propagates from transmitter to receiver through the background medium without the imbedded scatterers. For the radar return from a target in the presence of clutter, $\overline{\mu}_t$ corresponds to the response of the target. The fluctuation field $\overline{X}_f$ with zero mean is the scattered field due to the randomly distributed scatterers within the illuminated region. Normalizing the received power by the illuminated area A yields $\overline{X}$

$$\overline{X} = \overline{\mu} + \frac{1}{\sqrt{A}}\overline{X}_f \tag{18a}$$

$$\overline{\mu} = \frac{1}{\sqrt{A}}\overline{\mu}_t \tag{18b}$$

which is the direct generalization of (2). As the illuminated area A approaches infinity, the limiting distribution of $\overline{X}$ for the homodyned model is given by

$$P(\overline{X}) = \frac{1}{(2\pi)^{n/2}|\overline{\overline{C}}|^{1/2}} \frac{(2\alpha)^{n/4+\alpha/2}\left[(\overline{X}-\overline{\mu})^T \cdot \overline{\overline{C}}^{-1} \cdot (\overline{X}-\overline{\mu})\right]^{\alpha/2-n/4}}{2^{\alpha-1}\Gamma(\alpha)} \times K_{n/2-\alpha}\left(\sqrt{2\alpha}\left[(\overline{X}-\overline{\mu})^T \cdot \overline{\overline{C}}^{-1} \cdot (\overline{X}-\overline{\mu})\right]^{1/2}\right) \tag{19}$$

The other approach extending the K-distribution to the non-zero-mean case is to generalize the directional bias random walk model [15,17]. The received field $\overline{X}_{rec}$ (1) is again decomposed into the mean part and fluctuation part

$$\overline{X}_{rec} = N\overline{X}_{\mu} + \sum_{j=1}^{N}(\overline{X}_j - \overline{X}_{\mu}) \tag{20}$$

where in this case the $\overline{X}_{\mu}$ is the expected value of $\overline{X}_j$.

Now, we assume that we are able to scale both the mean and the variances of each step component by A or N_a. A similar scaling assumption was also made in [15,17]. Then, the normalized field will be given as

$$\overline{X} = \frac{1}{A}(N\overline{X}_{\mu}) + \frac{1}{\sqrt{A}}\sum_{j=1}^{N}(\overline{X}_j - \overline{X}_{\mu}) \tag{21}$$

The first term is the mean part and the second term corresponds to the fluctuation part of the measurement.

Then, assuming the negative binomial distribution for the number of scatterers, averaging the characteristic function of $\overline{X}$ over N, and letting the illuminated area A approach infinity, we have the characteristic function for $\overline{X}$

$$\Phi_{N_a}(\overline{k}) = \left[1 - i\frac{\overline{k}\cdot\overline{\mu}}{\alpha} + \frac{1}{2\alpha}\overline{k}^T\cdot\overline{\overline{C}}\cdot\overline{k}\right]^{-\alpha} \tag{22}$$

where

$$\overline{\mu} = \frac{N_a\overline{X}_{\mu}}{A} \tag{23}$$

and $\overline{\overline{C}}$ is given in (10) with

$$\overline{\overline{C}}_s = E\left[(\overline{X}_j - \overline{X}_{\mu})(\overline{X}_j - \overline{X}_{\mu})^T\right] \tag{24}$$

Equation (22) is a generalization of the directional bias random walk model [17]. The PDF corresponding to $\Phi_{N_a}(\overline{k})$ of (22) is given by

$$P(\overline{X}) = \frac{1}{(2\pi)^{n/2}|\overline{\overline{C}}|^{1/2}}\frac{\exp\left(\overline{\mu}^T\cdot\overline{\overline{C}}^{-1}\cdot\overline{X}\right)}{(1+\frac{y_{\mu}}{2\alpha})^{\alpha/4-n/8}}\frac{(2\alpha)^{n/4+\alpha/2}y^{\alpha/2-n/4}}{2^{\alpha-1}\Gamma(\alpha)} \times K_{n/2-\alpha}\left[\sqrt{2\alpha}\left(1+\frac{y_{\mu}}{2\alpha}\right)^{1/2}y^{1/2}\right] \tag{25}$$

where

$$y = \overline{X}^T \cdot \overline{\overline{C}}^{-1} \cdot \overline{X}$$

$$y_\mu = \overline{\mu}^T \cdot \overline{\overline{C}}^{-1} \cdot \overline{\mu}$$

which can be obtained by making use of the derivation of (11) as shown in appendix A.

If the mean vector $\overline{\mu}$ is set to zero, both the homodyned K-distribution (19) and directional biased K-distribution (25) degenerate to the zero-mean K-distribution (11). However, the physical scattering processes and scaling procedures assumed in the derivations of the two nonzero mean K-distributions are entirely different. For the homodyned approach, the mean part $\overline{\mu}$ represents the received field in the absence of imbedded scatterers. However, in the directional bias model, both the mean part and the fluctuating part are due to the scatterers, and the contribution of each scatterer to the mean part is completely coherent. The appropriate nonzero mean K-distribution for a real problem is therefore determined by the scattering process involved. In this regard Jakeman [17], after studying the expectation of intensity before averaging over N and scaling, concluded that the biased random walk did not correctly model the effects generated by weakly scattering media. The homodyned process, on the other hand, has been shown to be in excellent agreement with experimental data when a laser beam is scattered by a turbulent layer of air [13].

4.3 PDF of Normalized Zero-mean K-distributed Vector

Consider polarimetric measurements at three polarizations: HH, HV, and VV. In this case, we have a six-dimensional polarimetric feature vector $\overline{X}$

$$\overline{X} = \begin{bmatrix} x_1 \\ x_2 \\ x_3 \\ x_4 \\ x_5 \\ x_6 \end{bmatrix} = \begin{bmatrix} Re(HH) \\ Im(HH) \\ Re(HV) \\ Im(HV) \\ Re(VV) \\ Im(VV) \end{bmatrix} \tag{26}$$

The polarimetric vector is assumed now to be zero-mean K-distributed, as given by (11). In the following, the PDF of normalized polarimetric

data will be derived. The PDF for an n-dimensional feature vector is given in appendix D.

We choose the Euclidean norm $E = \sqrt{|HH|^2 + |HV|^2 + |VV|^2}$ as the normalization function and make the following transformation

$$Re(HH) = E\cos\phi\sin\theta\cos\phi_{hh} \tag{27a}$$
$$Im(HH) = E\cos\phi\sin\theta\sin\phi_{hh} \tag{27b}$$
$$Re(HV) = E\sin\phi\sin\theta\cos\phi_{hv} \tag{27c}$$
$$Im(HV) = E\sin\phi\sin\theta\sin\phi_{hv} \tag{27d}$$
$$Re(VV) = E\cos\theta\cos\phi_{vv} \tag{27e}$$
$$Im(VV) = E\cos\theta\sin\phi_{vv} \tag{27f}$$

The Jacobian of the above transformation is

$$J = E^5\cos\phi\sin\phi\cos\theta\sin^3\theta \tag{28}$$

Therefore, the joint PDF of E, θ, ϕ, ϕ_{hh}, ϕ_{hv}, and ϕ_{vv} is

$$P(E,\theta,\phi,\phi_{hh},\phi_{hv},\phi_{vv}) = E^5\cos\phi\sin\phi\cos\theta\sin^3\theta\,P(\overline{X}) \tag{29}$$

The PDF of normalized data is the marginal PDF of θ, ϕ, ϕ_{hh}, ϕ_{hv}, and ϕ_{vv}. It can be written as

$$\begin{aligned} P(\theta,\phi,\phi_{hh},\phi_{hv},\phi_{vv}) &= \int_0^\infty P(E,\theta,\phi,\phi_{hh},\phi_{hv},\phi_{vv})\,dE \\ &= \frac{\cos\phi\sin\phi\cos\theta\sin^3\theta}{\pi^3\left|\overline{\overline{C}}\right|^{1/2}}\left(\frac{\overline{X}^T\cdot\overline{\overline{C}}^{-1}\cdot\overline{X}}{E^2}\right)^{-3} \end{aligned} \tag{30}$$

where

$$\overline{\overline{C}} = E(\overline{X}\,\overline{X}^T) \tag{31}$$

and the second equality of (30) is obtained by substituting (11) and (29) into the integral and carrying out the integration.

If the I and Q components of each polarization are of equal variance and uncorrelated, the PDFs of the amplitude ratio and phase difference between HH and VV, which can be derived by integrating

(30) over θ and ϕ_{hv}, are given as [1,3],

$$P(r) = 2\gamma(1-|\rho|^2)\frac{r(\gamma+r^2)}{[(\gamma+r^2)^2 - 4\gamma r^2|\rho|^2]^{3/2}} \tag{32a}$$

$$P(\phi) = \frac{(1-|\rho|^2)}{2\pi}\left\{\frac{(1-|\rho|^2\cos^2\phi)^{1/2} + |\rho|\cos\phi\,[\pi - \cos^{-1}(|\rho|\cos\phi)]}{(1-|\rho|^2\cos^2\phi)^{3/2}}\right\} \tag{32b}$$

where

$$r = \frac{|VV|}{|HH|} \tag{33a}$$

$$\phi = \phi_{hh} - \phi_{vv} - \phi_\rho \tag{33b}$$

and γ, $|\rho|$, and ϕ_ρ are related to the variances and complex covariance of HH and VV by

$$\gamma = \frac{<|VV|^2>}{<|HH|^2>} \tag{34a}$$

$$|\rho|\exp(i\phi_\rho) = \frac{<HH\;VV^*>}{\sqrt{<|HH|^2><|VV|^2>}} \tag{34b}$$

By replacing γ, $|\rho|$, and ϕ_ρ with e, $|\beta|$, and ϕ_β, respectively, where

$$e = \frac{<|HV|^2>}{<|HH|^2>} \tag{35a}$$

$$|\beta|\exp(i\phi_\beta) = \frac{<HH\;HV^*>}{\sqrt{<|HH|^2><|VV|^2>}} \tag{35b}$$

(32a) and (32b) are transformed into the PDFs for the ratio $r = |HV|/|HH|$ and phase difference $\phi_{hh} - \phi_{hv} - \phi_\beta$, respectively. For simplicity, the following notations will be used.

$$\phi_{hhvv} = \phi_{hh} - \phi_{vv} - \phi_\rho \tag{36a}$$

$$\phi_{hhhv} = \phi_{hh} - \phi_{hv} - \phi_\beta \tag{36b}$$

Note that the probability density function (30) of the normalized data is independent of the parameter α. This result also holds for an n

dimensional K-distributed feature vector, as shown in appendix D. A similar observation was made in [16] where the probability density function of total phase was shown to be independent of α. In this section, we prove the more general result that the joint probability density of the ratios of amplitudes and relative phases of all polarizations is independent of α. We can understand this phenomenon by the following reasoning. The K-distribution arises from fluctuations in the number of scatterers which are characterized by the parameter α, and that parameter manifests its effects only on the absolute amplitude of the polarimetric data. Relative magnitudes and phases are completely characterized by the covariance matrix of the polarimetric return from each scatterer, $\overline{\overline{C}}_s$, given in (8). Thus, when the absolute amplitude information contained in the polarimetric data is taken away, the joint probability density function of the normalized polarimetric data is independent of α.

4.4 Results and Discussion

Four sets of radar measurements including JAWS data, Traverse City data, Mt. Shasta data, and DLR data are analyzed and discussed in this section. JAWS data are obtained from MIT Lincoln Laboratory, Traverse City and Mt. Shasta data are from JPL, and DLR data are from the German Aerospace Research Establishment. JAWS and Mt. Shasta data are in the form of polarimetric scattering matrix, whereas DLR data are the recorded amplitude of VV returns. Traverse City data consist of two images corresponding to two neighboring sites, where one of the images is in the form of one-look Mueller matrix and the other has the form of scattering matrix. Sample areas of typical clutter classes have been analyzed. The sampled areas have been chosen to have sufficient number of pixels to ensure the significance of the distribution statistics.

Comparisons will be presented between measured normalized intensity moments and cumulative density functions (CDF) of quantities including $|HH|$, $|HV|$, $|VV|$, $|VV|/|HH|$, $|HV|/|HH|$, ϕ_{hhvv}, and ϕ_{hhhv}, and those of the zero-mean K-distribution. Expected normalized intensity moments were calculated using (15). The parameter α is then estimated by equating (16) with the measured $I^{(2)}$ which is set equal to the average of $I^{(2)}_{HH}$, $I^{(2)}_{HV}$, and $I^{(2)}_{VV}$. Subsequently, expected K-distributions (12) were calculated by using the estimated α. Param-

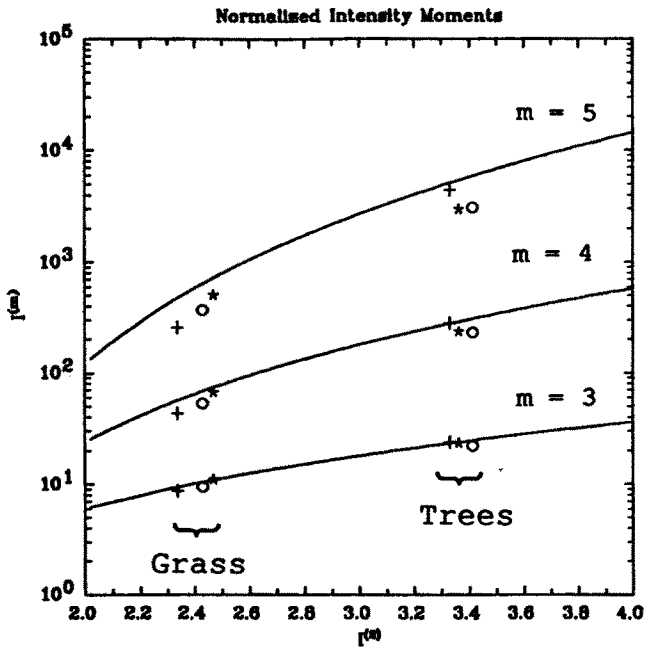

Figure 4.1 Higher-order normalized intensity moments versus second-order normalized intensity moment of JAWS polarimetric data. The solid curves are the theoretical results of K-distribution. Two clutter classes, trees and grass, are shown. o, +, and * represent the measured HH, HV, and VV returns, respectively.

eters, e, γ, $|\rho|$, $|\beta|$, ϕ_ρ, and ϕ_β, required in evaluating the expected PDFs of amplitude ratio (32a) and phase difference (32b), are related to the measured covariances of polarimetric data by (34) and (35). Note that in arriving at (12), (15), and (32), I and Q components were assumed to be zero mean, uncorrelated, and of equal variances. Scattering matrix data of JAWS, Traverse City, and Mt. Shasta support these assumptions.

a. JAWS Data

The JAWS data were measured at 35 GHz with the incident angle of approximately 82° [21]. The ground resolution is about 1 foot in range and 100 feet in azimuth. Data from two clutter classes, grass and trees, are illustrated in Figs. 4.1 to 4.5. Higher-order normalized intensity moments are plotted versus second-order normalized inten-

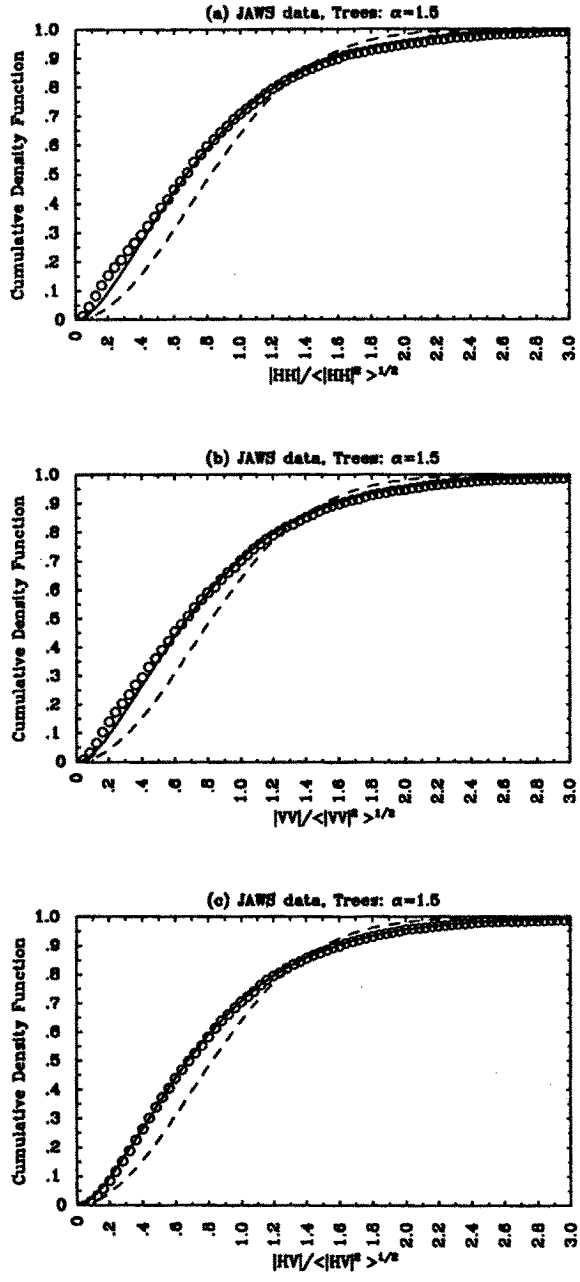

Figure 4.2 CDF versus (a) $|HH|/<|HH|^2>^{1/2}$, (b) $|VV|/<|VV|^2>^{1/2}$, and (c) $|HV|/<|HV|^2>^{1/2}$, of trees in JAWS data. The dashed line represents Rayleigh distribution. o represents experimental data. The solid curve represents K-distribution with $\alpha = 1.5$.

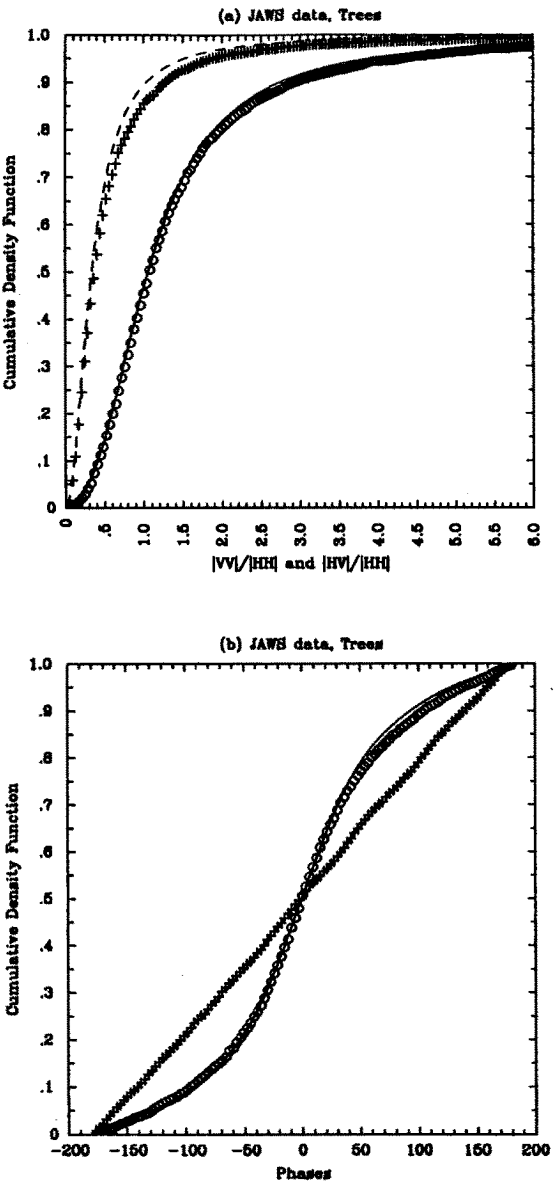

Figure 4.3 CDF versus (a) $|VV|/|HH|$ and $|HV|/|HH|$ and (b) ϕ_{hhvv} and ϕ_{hhhv} of trees in JAWS data. o represents measured $|VV|/|HH|$ or ϕ_{hhvv}. + represents measured $|HV|/|HH|$ or ϕ_{hhhv}. Solid and dashed curves correspond to expected K-distributions.

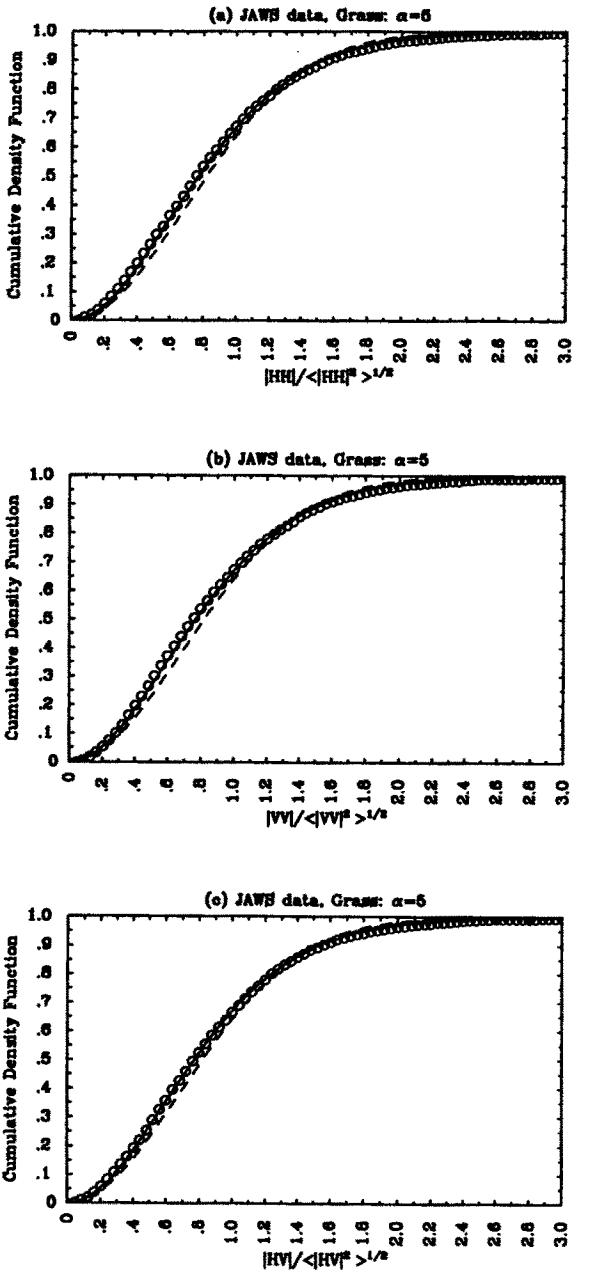

Figure 4.4 CDF versus (a) $|HH|/<|HH|^2>^{1/2}$, (b) $|VV|/<|VV|^2>^{1/2}$, and (c) $|HV|/<|HV|^2>^{1/2}$, of grass field in JAWS data. o represents experimental data. The solid curve represents K-distribution with $\alpha = 5$.

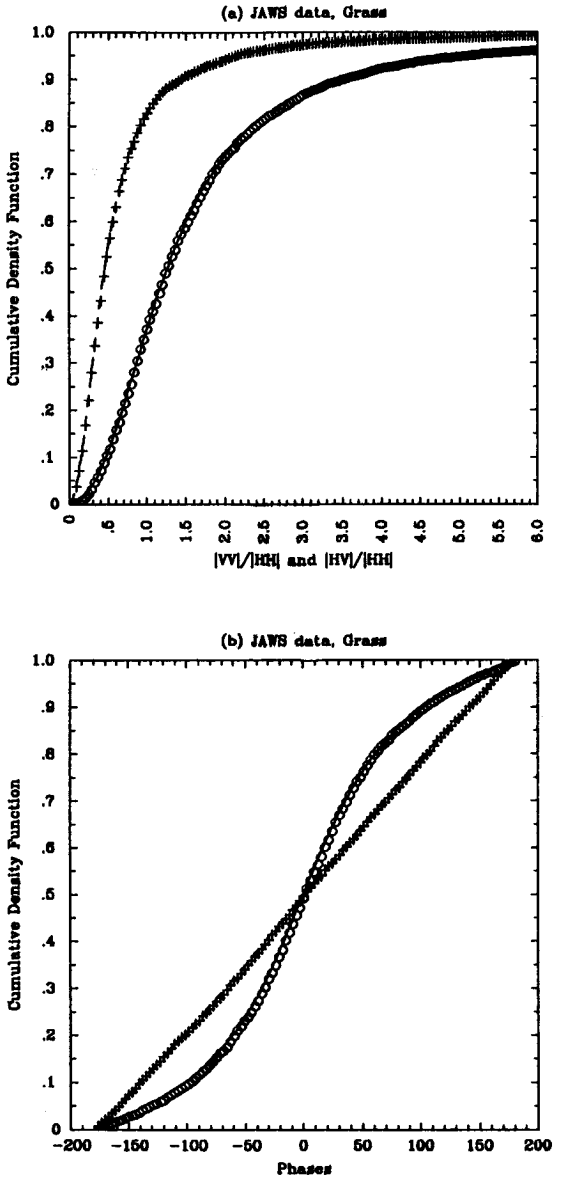

Figure 4.5 CDF versus (a) $|VV|/|HH|$ and $|HV|/|HH|$ and (b) ϕ_{hhvv} and ϕ_{hhhv} of grass field in JAWS data. o represents measured $|VV|/|HH|$ or ϕ_{hhvv}. + represents measured $|HV|/|HH|$ or ϕ_{hhhv}. Solid and dashed curves correspond to expected K-distributions.

sity moment in Fig. 4.1. The measured normalized intensity moments (14) for HH, HV, and VV polarizations are represented by $\circ$, $+$, and $*$, respectively. The solid curves are the theoretical higher-order normalized intensity moments of the K-distribution. The parameter α for grass is estimated to be approximately 5, based on (16). The parameter α for the tree region is approximately 1.5. This value is consistent with experimental data shown in [10]. For the tree region, the measured CDF of normalized amplitudes (13) for the polarizations HH, VV, and HV are shown in Figs. 4.2(a), 4.2(b), and 4.2(c), respectively. The parameter $\alpha = 1.5$ is used to evaluate the K-distribution for all polarizations. The Rayleigh distribution is also shown for comparison. The comparisons between (32) and measured CDFs of amplitude ratios $|VV|/|HH|$ and $|HV|/|HH|$, and phase differences ϕ_{hhvv} and ϕ_{hhhv}, are shown in Figs. 4.3(a) and 4.3(b). For the tree region, the measured parameters e, γ, $|\rho|$, $|\beta|$, ϕ_ρ, and ϕ_β, are 0.122, 1.147, 0.576, 0.0625, $-3.29°$, and $-21.24°$, respectively. Similar CDF data for amplitudes, amplitude ratios, and phase differences are shown in Figs. 4.4 and 4.5 for the grass region, where the parameter $\alpha = 5$ has been used to evaluate the K-distribution. It can be seen that the experimental data are in very good agreement with the expected K-distributions.

b. Traverse City Data

Traverse City data are L-band polarimetric SAR images of two consecutive sites of a region near Traverse City, Michigan, and were measured with the incident angle varying from approximately 25° at near range to 55° at far range [6]. Each pixel represents approximately 10 m in range and 3 m in azimuth on the ground. We chose a corn field from one of the SAR images and three homogeneous clutter patches (a lake, a bare field, and a forest) from the other image to study the normalized intensity moments of the polarimetric returns. Corn field data are in the form of Mueller matrix, whereas the others are in the form of scattering matrix data. The results are shown in Fig. 4.6. It can again be seen that the experimental data agree very well with the expected K-distributions. The parameter α for the corn field is estimated to be approximately 1.4. The CDFs of the amplitudes of HH and VV returns from the corn field are shown in Figs. 4.7(a) and 4.7(b), respectively. They are in good agreement with a K-distribution with the parameter $\alpha = 1.4$. As observed from the Traverse City images classified into dif-

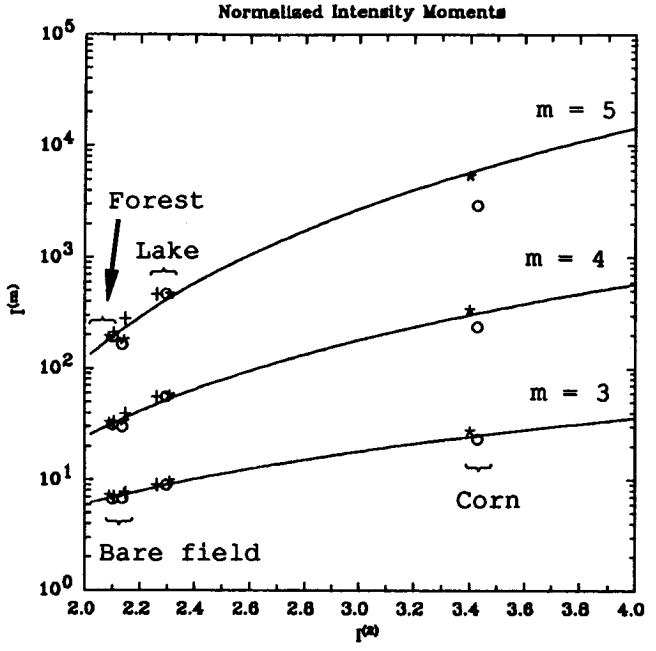

Figure 4.6 Higher-order normalized intensity moments versus second-order normalized intensity moment of Traverse City SAR polarimetric image. The solid curves are the theoretical results of K-distribution. Four clutter classes: corn field, lake, forest, and bare field, are shown. o, +, and * represent the measured HH, HV, and VV returns, respectively.

ferent terrain types in Figures 6.5, 6.6, and 6.12 in Chapter 6, there are some color coded red and yellow parallel stripes appearing in the corn field region. Note that any observable stripes must have width greater than the size of one resolution cell. Red represents corn and yellow corresponds to bare field. This indicates that this selected corn field area is in fact a mixture of bare fields and corn fields. This may explain the large power fluctuation (small α) of this area as opposed to the crop land in DLR data set. The CDFs of $|VV|/|HH|$ and ϕ_{hhvv} are shown in Figs. 4.8(a) and 4.8(b), respectively. The measured parameters, γ, $|\rho|$, and ϕ_ρ, are 1.393, 0.518, and $-67.55°$, respectively. It can be seen that the CDF of measured $|VV|/|HH|$ ratios almost overlays exactly that predicted by (32a). For the lake, bare field, and forest, the CDFs of measured $|HH|$, $|HV|$, and $|VV|$, though not shown, were very close to the Rayleigh distribution. The CDFs for measured amplitude ratios and phase differences, also not shown in this chapter, overlay

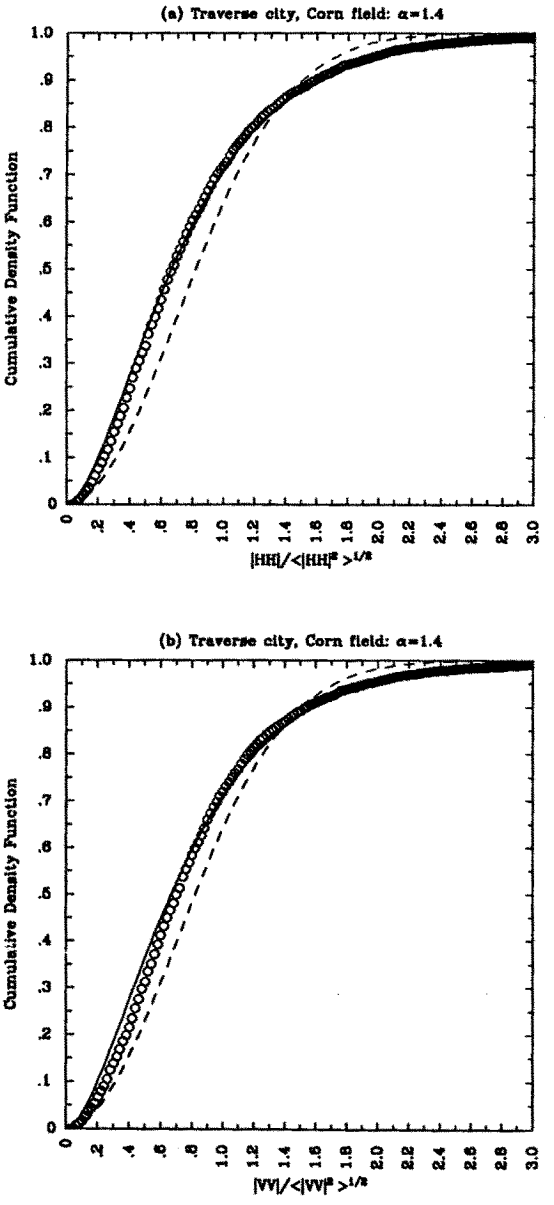

Figure 4.7 Cumulative density function versus (a)$|HH|/<|HH|^2>^{1/2}$, and (b) $|VV|/<|VV|^2>^{1/2}$, of the corn field in Traverse City data. o represents experimental data. The solid curve represents K-distribution with $\alpha = 1.4$.

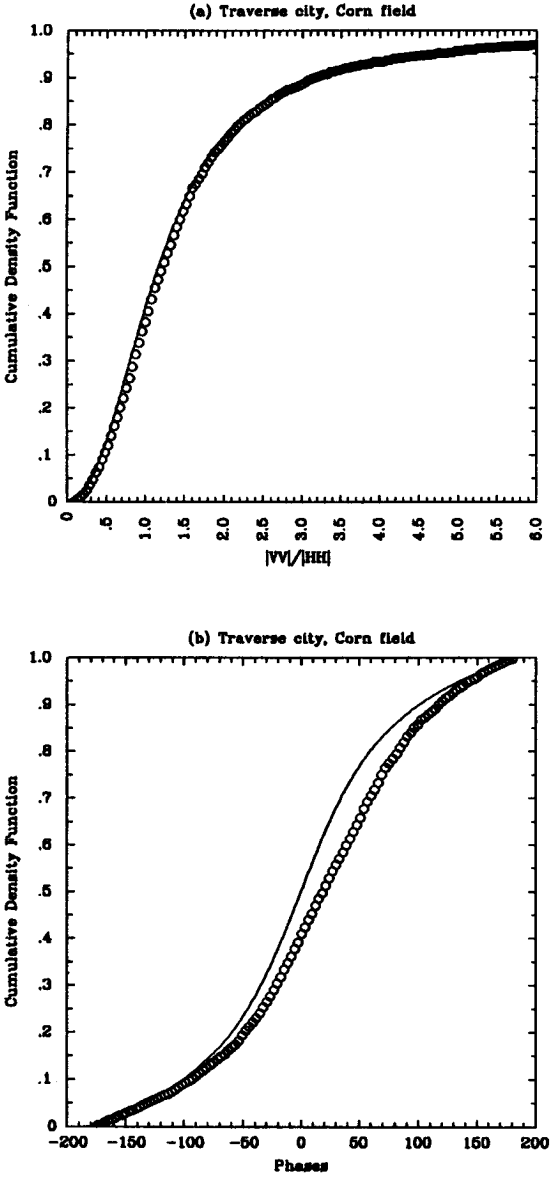

Figure 4.8 CDF versus (a) $|VV|/|HH|$ and (b) ϕ_{hhvv} of the corn field in Traverse City data. o represents measured $|VV|/|HH|$ or ϕ_{hhvv}. Solid and dashed curves correspond to expected K-distributions.

almost exactly those calculated by using (32). The α's inferred from Traverse City SAR data for the lake, bare field, and forest are approximately 6.7, 15.4, and 20.0, respectively. When α approaches infinity or $I^{(2)}$ approaches 2, the expected K-distribution function approaches Gaussian distribution. Note that the CDF of JAWS grass field data, where $\alpha = 5$, are very close to Gaussian. Thus, the PDFs of Traverse City polarimetric data from the lake, bare field, and forest are approximately Gaussian. However, the corn field data are far from Gaussian and clearly K-distributed.

Note that the PDFs of JAWS tree data are K-distributed, whereas that of Traverse City forest data are Gaussian. Because the K-distribution has larger high-order normalized intensity moments (15), this indicates that the Traverse City data have less spatial variation than the JAWS data. This may be due to the different types of trees in the two cases and the trees near Traverse City (JPL data) are more homogeneous and well developed than those in the JAWS site. The different distributions may also be attributed to differences in the radar look angle and beam footprint between these two sets of data. The resolution of the Traverse City SAR image is about 30 square meters which has larger spatial averaging effect than the 100 square feet resolution of the JAWS data. Also, the shadowing effect is not significant in the Traverse City data (45° incidence) unlike the JAWS data where the incident angle was 82° . All of the above factors will result in less spatial variation of scattering coefficients for the Traverse City data, thus making the SAR data from a forest near Traverse City appear more Gaussian.

c. Mt. Shasta Data

Mt. Shasta data contain simultaneously measured C-, L- and P-band polarimetric SAR images of an area in Mt. Shasta in northern California [24]. The images cover an area of about 12 km by 5 km and each pixel represents 6.662 m in slant range and 3.03 m in azimuth on the ground. The imaged Mt. Shasta site contains some forested areas with conifers and some hardwoods and a burned region having smaller trees (35 meters versus 45 meters for the the undamaged area) [24]. Data are plotted and compared with K-distribution for two clutter classes: forested area and burned area.

Figure 4.9 illustrates the averaged normalized intensity moment $I^{(2)}$ and the estimated α versus wavelength for these two selected clut-

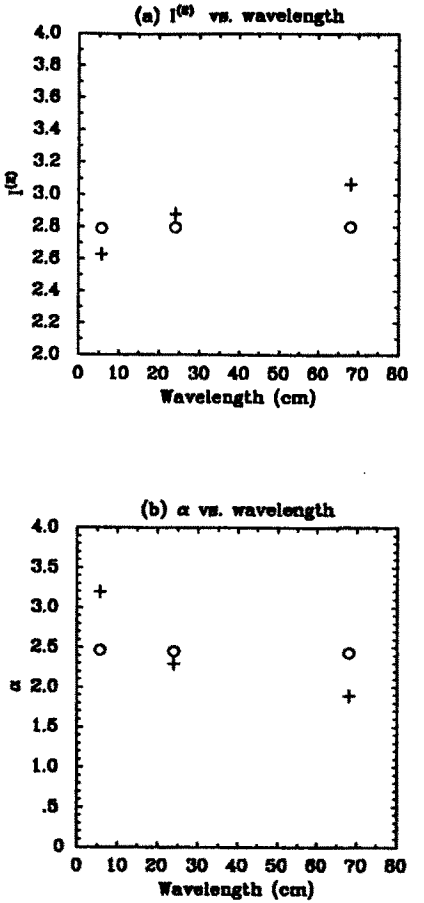

Figure 4.9 Measured (a) $I^{(2)}$ and (b) α versus wavelength at C, L, and P bands. o and + represent data from forested and burned areas, respectively.

ter classes. The parameter α is estimated to be 2.49 at C-band, 2.47 at L-band, and 2.46 at P-band for the undamaged forest; whereas α is estimated to be 3.2, 2.3, and 1.9 for C-, L-, and P-bands, respectively, for the burned forest area. It appears that the clutter power variation, $I^{(2)}$, is larger toward the lower frequency band for the burned region, whereas it remains essentially constant for the healthy forested area at all frequency bands. This can be due to the differing penetration effects between these two regions.

Larger clutter fluctuation $I^{(2)}$ at the lower frequency band could be due to the fact that electromagnetic waves at different frequencies

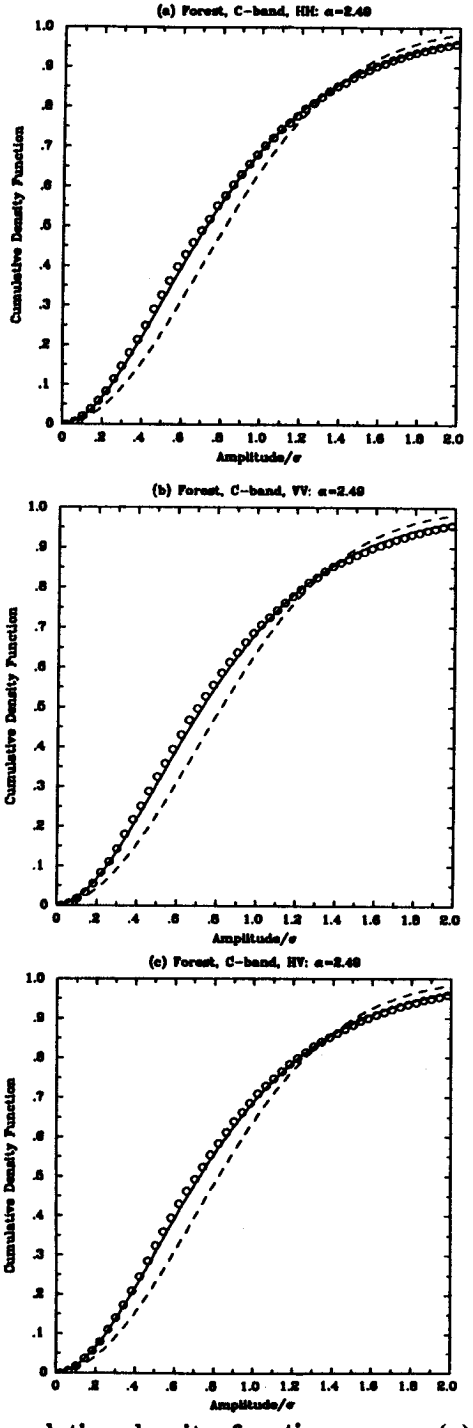

Figure 4.10 Cumulative density function versus (a) $|HH|$, (b) $|VV|$, and (c) $|HV|$ for C-band SAR image of Mt. Shasta forests. o represents experimental data. The dashed line represents Rayleigh distribution and the solid curve corresponds to K-distribution with $\alpha = 2.49$.

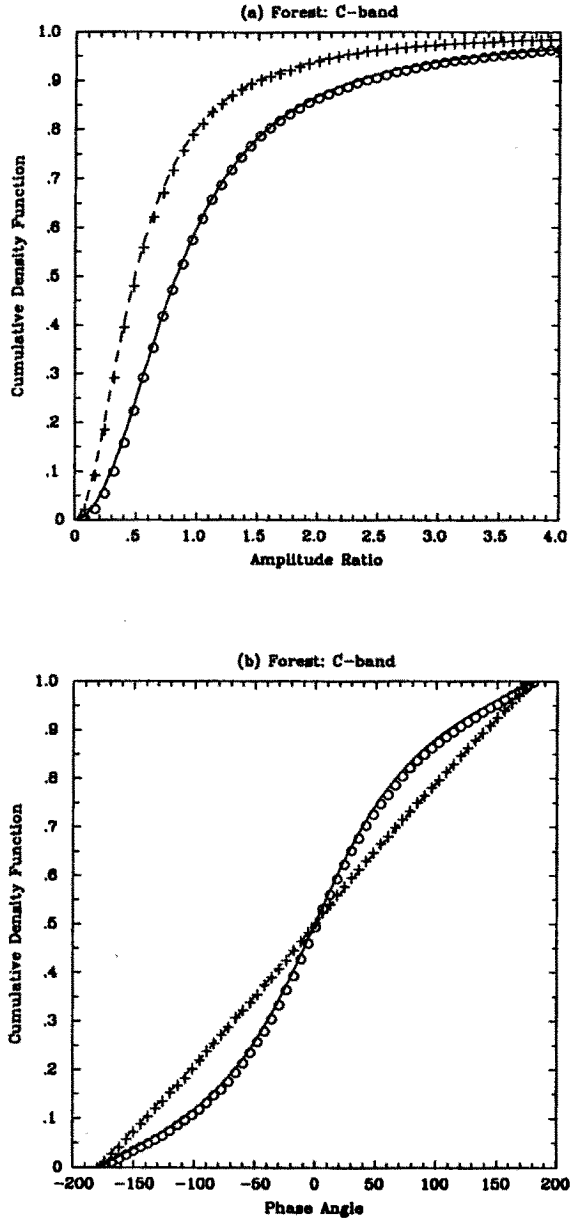

Figure 4.11 Cumulative density function versus (a) $|VV|/|HH|$ and $|HV|/|HH|$ and (b) ϕ_{hhvv} and ϕ_{hhhv} for C-band SAR image of Mt. Shasta forests. o represents measured $|VV|/|HH|$ or ϕ_{hhvv}. + represents measured $|HV|/|HH|$ or ϕ_{hhhv}. Solid and dashed curves correspond to expected K-distributions.

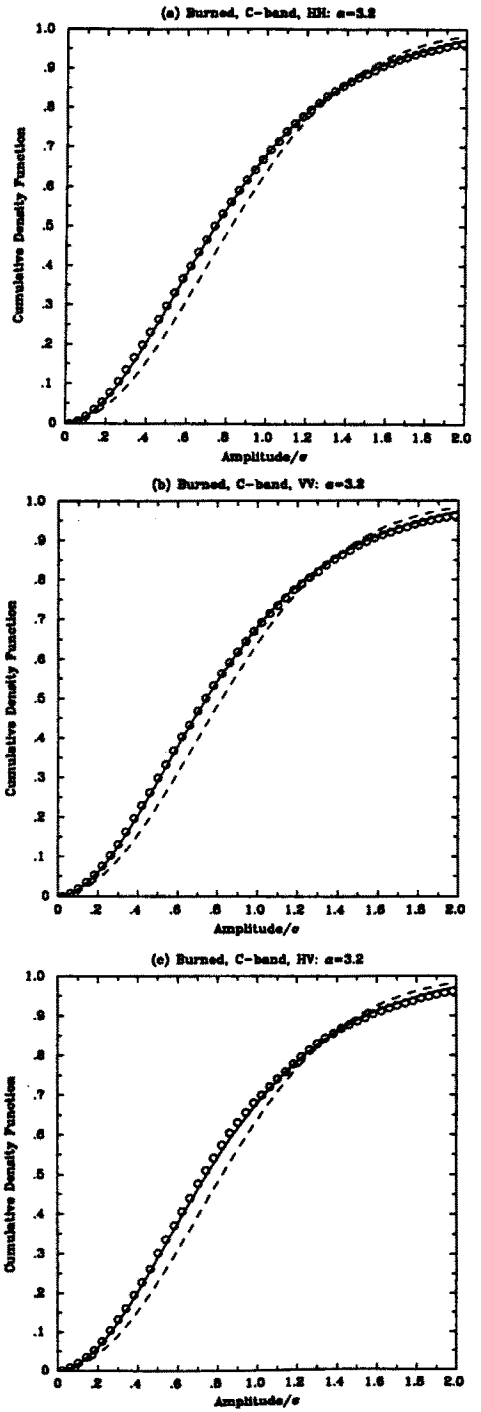

Figure 4.12 Cumulative density function versus (a) $|HH|$, (b) $|VV|$, and (c) $|HV|$ for C-band SAR image of Mt. Shasta burned area. o represents experimental data. The dashed line represents Rayleigh distribution and the solid curve represents K-distribution with $\alpha = 3.2$.

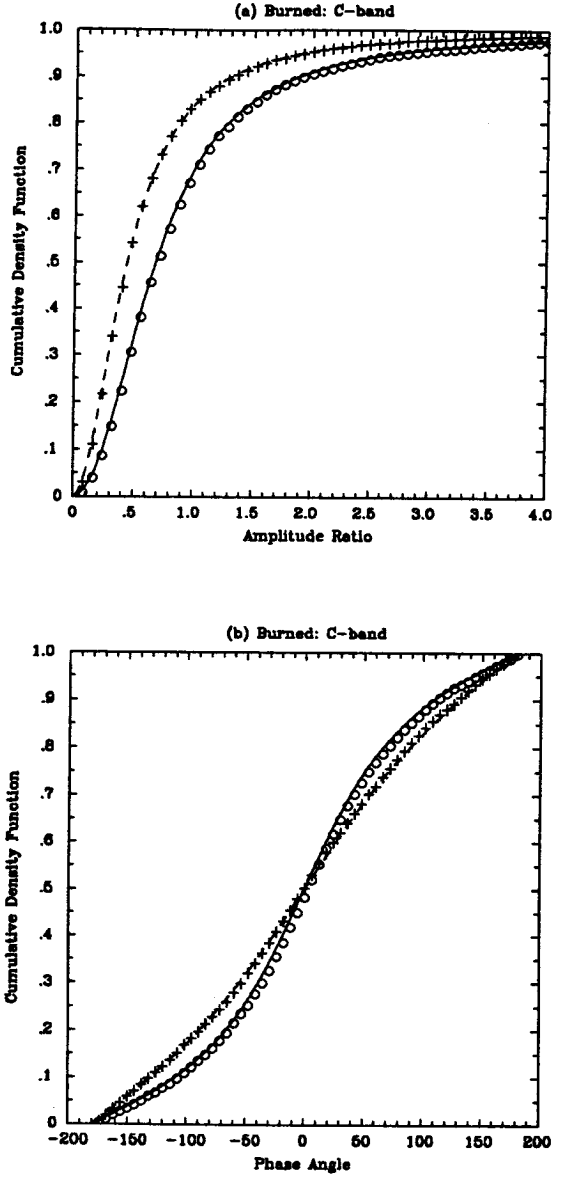

Figure 4.13 Cumulative density function versus (a) $|VV|/|HH|$ and $|HV|/|HH|$ and (b) ϕ_{hhvv} and ϕ_{hhhv} for C-band SAR image of Mt. Shasta burned area. o represents measured $|VV|/|HH|$ or ϕ_{hhvv}. + represents measured $|HV|/|HH|$ or ϕ_{hhhv}. Solid and dashed curves correspond to expected K-distributions.

experience different penetration depths, and therefore the resulting scattering effects differ. At burned forest area, waves at C-band may remain within the upper crown region, while the P-band waves may penetrate into the lower crown region and probably reach the trunk and underlying soil regions where the scatterers are in general less homogeneously distributed. As a result, the clutter fluctuation at the lower frequency band increases. However, the healthy forest may be so dense that the waves at all frequency bands remain within the upper crown region. Hence the same scattering effects are observed for the healthy forest area. However, the frequency dependence of α needs to be further studied, since the ground truth data were insufficient for the data analyzed in this paper.

The measured CDFs of amplitude, phase difference, and amplitude ratios have been computed for both clutter classes and are all in very good agreement with the expected K-distribution at all frequency bands. The corresponding curves for the K-distribution were computed from (12) and (32) by selecting a parameter α and a covariance matrix $\overline{\overline{C}}$ that match the experimental data at each frequency band. Figures 4.10–4.13 illustrate the C-band data from the selected areas. The measured CDFs of $|HH|$, $|HV|$, and $|VV|$ are shown in Figs. 4.10 and 4.12 where σ represents the measured standard deviation of signal amplitudes over the selected area. The Rayleigh distribution is also included for comparison. The calculated and measured CDFs of amplitude ratios $|VV|/|HH|$ and $|HV|/|HH|$, and phases ϕ_{hhvv} and ϕ_{hhhv} are shown in Figs. 4.12 and 4.14 for both clutter classes. It can be seen that the experimental data are in good agreement with the expected K-distribution.

d. DLR Data

The data from DLR [25,26] are a very high resolution VV image of a farm land with the incident angle varying from 33° at near range to 67° at far range. The ground resolution is 2 meters in range and 0.5 meters in azimuth, and the operating frequency is centered at 5.3 GHz (C-band). The imaged area contains mostly cultivated crop lands, a few lakes, and a forested area. Note that $I_{VV}^{(2)}$ is used for the estimation of α. The measured α for the selected crop land and lake are 20 and 7, respectively, and the measured CDFs are in very good agreement with the Rayleigh distribution. However, the measured α for the forested

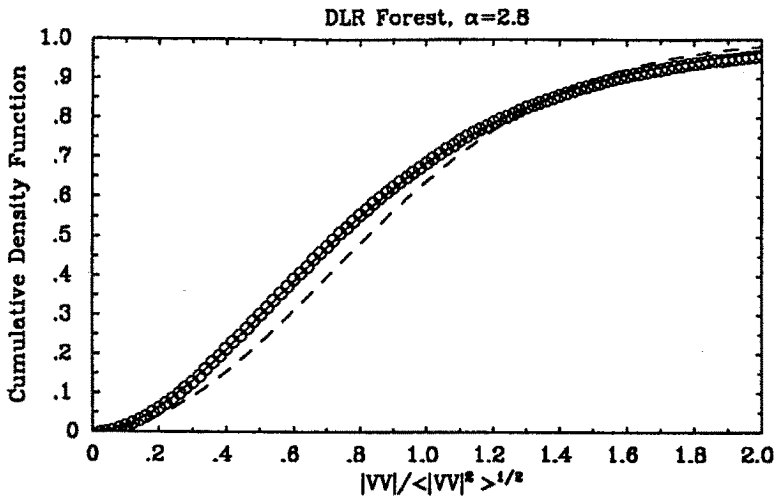

Figure 4.14 Cumulative density function versus $|VV|/ < |VV|^2 >^{1/2}$ for forested area data obtained from DLR. o represents experimental data. The dashed line represents Rayleigh distribution and the solid curve represents K-distribution with $\alpha = 2.8$.

area is 2.8, and the CDF data plotted in Fig. 4.14 are in good agreement with the K-distribution.

e. Effects of Radar Calibration

In this section, the effects of polarimetric radar miscalibration and radar characteristics at different frequencies will be addressed. For the polarimetric miscalibration, the presence of the cross-talk and channel imbalance makes the measured scattering (covariance) matrix elements become a linear combination of the true scattering (covariance) matrix elements. Hence, just like the measured polarimetric data shown in this paper having a K-distribution, the original polarimetric data will also be K-distributed except having a different covariance matrix.

Another common concern is whether the observed statistics for the cross-polarization HV is due to the polarization cross-talk. We can expect that if HV is due to the cross-coupling from HH or VV channels, then HV should be highly correlated with HH and VV. However, the experimental data show that the measured correlation coefficient is small between HV and HH or VV ranging from 0.03 to 0.2 except

for the L-band images of the undamaged forest (≈ 0.3). Note that the correlation coefficient, defined as the magnitude of the covariance normalized by the standard deviation, is one for complete correlation and zero for no correlation. The fact that the correlation coefficient is small indicates that the effect of cross-talk was small in measured HV. As seen in Fig. 4.11(b) the fairly small correlation between HH and HV (0.05) results in an almost uniform distribution for the measured ϕ_{hhhv} as compared with the measured distribution for ϕ_{hhvv} (0.4 correlation between HH and VV).

The remaining issue is whether the observed frequency behaviour of α is due to the radar characteristics at different frequency bands. As indicated before, α inverted from the normalized intensity moment $I^{(2)}$ characterizes the spatial variation of the power. Hence, fluctuations of both terrain clutter and variations due to the system misfunction will contribute to the measured power variation. However, it is reasonable to believe that the radar system parameters, including the radar transmitted power, the antenna gains, and the platform motions at each frequency band remain essentially constant within a short time period while the radar is imaging over each sample area. Therefore, the observed K-distribution in this chapter should be the result of terrain clutter fluctuations.

4.5 Summary

The multivariate K-distribution has proven to be useful in characterizing the distribution of polarimetric radar returns from most terrains. This indicates that the terrain clutter fluctuations in a SAR image of a given area result from (1) the speckle fluctuations and (2) the intrinsic spatial variation. The parameter α can be consequently useful to characterize the terrain types with respect to their spatial homogeneity. When α approaches infinity the terrain is homogeneous and the clutter approaches Gaussian distributed speckle (Rayleigh distribution for amplitude). For a given terrain type, the homogeneity characteristics depend on factors including the spatial resolution, the frequency, and the polarization. Spatial resolution may be the most important factor. A terrain may appear homogeneous at coarse resolution and heterogeneous at resolution finer than a threshold value related to the internal structure of the terrain scattering elements. Most mature forests may present an intrinsic return fluctuation in ad-

dition to speckle variation at resolution less than a value (say 100 m^2) related the crown size or tree spacing. At coarser resolution (e.g., 30 m by 30 m), the forest patches will have only speckle fluctuations. In the cases of agricultural fields or grass lands, they will appear homogeneous with respect to the resolution of most current airborne and spaceborne systems (> 3 m).

The results obtained with the forested areas are consistent with the above reasoning. The pixels values are K-distributed and α values are low among the cases studied ($\alpha = 1.5$ for JAWS data, 2 to 3 for Mt. Shasta data, 2.8 for DLR data). Viewed by SAR systems with spatial resolution less than 100 m^2, the forests appeared as heterogeneous areas. Crops and bare fields are Rayleigh distributed. Their α values are high, 15 (Traverse City) and 20 (DLR), which denotes homogeneous areas. Lake and grass samples are also close to Rayleigh distributions. The selected corn field and forest in Traverse City are exceptions.

The frequency, incident angle, and polarization are the other factors which affect the terrain spatial homogeneity. As stated before, lower frequencies and smaller angles of incidence correspond to deeper penetration within the medium. In addition, the penetration depth, and consequently, the scattering sources may vary as a function of the polarization if the medium is anisotropic.

The results from multifrequency data of Mt. Shasta area support the expected effect of the frequency on the parameter α. However, further work remains to be done to explore the effect of the polarization, the incident angle, together with the effect of the frequency. It can be expected that the parameter α and a covariance matrix of the K-distribution resulting from multifrequency, multipolarization and data will be a promising tool for terrain cover identification.

Appendix A: PDF of Multivariate K-distributed n-Dimensional Vector

The PDF of the resultant vector $\overline{X}$ can be obtained by taking the inverse Fourier transform of the characteristic function (9), i.e.,

$$P(\overline{X}) = \frac{1}{(2\pi)^n} \int d^n\overline{k} \frac{e^{-i\overline{k}\cdot\overline{X}}}{\left[1 + \frac{1}{2\alpha}\overline{k}^T \cdot \overline{\overline{C}} \cdot \overline{k}\right]^\alpha} \tag{A1}$$

In order to derive an explicit formula for $P(\overline{X})$, we use a transformation matrix $\overline{\overline{U}}$ such that the covariance matrix $\overline{\overline{C}}$ is diagonalized.

$$\overline{\overline{\Lambda}} = \overline{\overline{U}}^T \cdot \overline{\overline{C}} \cdot \overline{\overline{U}} \tag{A2}$$

where the matrix elements of $\overline{\overline{\Lambda}}$ are

$$[\overline{\overline{\Lambda}}]_{ij} = \lambda_i \delta_{ij} \tag{A3}$$

For convenience, we assume all eigenvalues λ_i, $i = 1, 2, \cdots, n$ are positive. After making the following transformations

$$\overline{z} = \overline{\overline{\Lambda}}^{-1/2} \cdot \overline{\overline{U}}^T \cdot \overline{X} \tag{A4a}$$

$$\overline{w} = \overline{\overline{\Lambda}}^{1/2} \cdot \overline{\overline{U}}^T \cdot \overline{k} \tag{A4b}$$

we obtain the following two equalities

$$\overline{z}^T \cdot \overline{z} = \overline{X}^T \cdot \overline{\overline{C}}^{-1} \cdot \overline{X} \tag{A5a}$$

$$\overline{w}^T \cdot \overline{z} = \overline{k}^T \cdot \overline{X} \tag{A5b}$$

Substituting (A5) into (A1) and transforming the integration variable $\overline{k}$ into $\overline{w}$, we have

$$\begin{aligned} P(\overline{X}) &= \frac{1}{(2\pi)^n |\overline{\overline{C}}|^{1/2}} \int d^n\overline{w} \frac{e^{-i\overline{w}^T \cdot \overline{z}}}{\left[1 + \frac{1}{2\alpha}\overline{w}^T \cdot \overline{w}\right]^\alpha} \\ &= \frac{1}{(2\pi)^{n/2} |\overline{\overline{C}}|^{1/2}} \frac{(2\alpha)^{n/4+\alpha/2} (\overline{z}^T \cdot \overline{z})^{\alpha/2-n/4}}{2^{\alpha-1}\Gamma(\alpha)} \\ &\quad \times K_{n/2-\alpha}\left[\sqrt{2\alpha}\,(\overline{z}^T \cdot \overline{z})^{1/2}\right] \end{aligned} \tag{A6}$$

Finally substituting (A5a) into (A6), we arrive at the PDF (11) for $\overline{X}$.

Appendix B: Alternative Derivation of Multivariate K-distribution

By assuming the Gaussian statistics for $\overline{X}$ and a large N_a, an alternative derivation of the multivariate K-distribution will be given in this appendix. The final result will provide a useful simulation model for the multivariate K-distributed random vector.

With the asymptotic expansion of gamma function for large argument,

$$\Gamma(z) \approx z^{z-1/2}e^{-z}\sqrt{2\pi} \tag{B1}$$

it can be shown that for large N_a and N, the negative binomial distribution (2) can be approximated by

$$\begin{aligned} P(N)\Delta N \approx \frac{1}{\Gamma(\alpha)}e^{1-\alpha}\alpha^{\alpha}\left(\frac{N}{N_a}\right)^{\alpha}\frac{(1+\alpha/N)^N}{(1+\alpha/N_a)^N}\frac{(1+\alpha/N)^{\alpha}}{(1+\alpha/N_a)^{\alpha}} \\ \times (1+1/N)^{-N}\sqrt{\frac{N+1}{N+\alpha}}\frac{1}{N+1}\Delta N \end{aligned} \tag{B2}$$

where $\Delta N = 1$. Thus,

$$P(N)\Delta N \approx \frac{1}{\Gamma(\alpha)}\alpha^{\alpha}\left(\frac{N}{N_a}\right)^{\alpha}\exp(-\frac{\alpha N}{N_a})\frac{N_a}{N}\Delta\left(\frac{N}{N_a}\right) \tag{B3}$$

Introducing the variable

$$\mu = N/N_a \tag{B4}$$

then (B3) can be written as

$$\begin{aligned} P(N)\Delta N &= P(\mu)d\mu \\ &= \frac{\alpha^{\alpha}\mu^{\alpha-1}}{\Gamma(\alpha)}\exp(-\alpha\mu)d\mu \end{aligned} \tag{B5}$$

It can be readily identified that $P(\mu)$ is a gamma probability density function for the continuous random variable μ, which may also be regarded as the continuum limit of the corresponding negative binomial distribution with large N_a and N.

We now let the number N be fixed and approaches infinity. Then, by the central limit theorem, the statistics of the polarimetric return

(1) can be approximated as Gaussian

$$P(\overline{X}|N) = \frac{1}{(2\pi)^{n/2}\left|\mu\overline{\overline{C}}\right|^{1/2}} \exp\left[-\frac{\overline{X}^t \cdot (\mu\overline{\overline{C}})^{-1} \cdot \overline{X}}{2}\right] \tag{B6}$$

where $\overline{\overline{C}}$ is given in (4) and μ is defined by (B4).

Averaging the above conditional Gaussian distribution over the negative binomial distribution at large N and N_a

$$\sum_N P(\overline{X}|N)P(N) \approx \int_0^\infty d\mu P(\overline{X}|N)P(\mu) \tag{B7}$$

The integration of the last integral can be carried out exactly [14] and gives rise to the multivariate K-distribution (6).

The above result indicates that the K-distributed random vector $\overline{X}$ can be considered as a conditional Gaussian random vector with the absolute radar cross section varying as a Gamma random variable. This model has been termed as the product model [18]. This interpretation can be used to generate the K-distribution in the following way: first generate a gamma random number μ with a given parameter α and then generate a Gaussian random vector $\overline{X}$ according to the covariance matrix $\mu\overline{\overline{C}}$.

Appendix C: Joint Moments of Multivariate K-distributed n-Dimensional Vector

For the zero mean random walk, the moments of the resultant vector can be easily calculated by taking the partial derivatives of the characteristic function (9) and letting $\overline{k}$ equal zero. Two useful joint moments are given as follows with $E(\cdot)$ denoting the expectation of the argument.

$$E(x_1 x_2 \cdots x_{2m}) = \frac{\Gamma(\alpha+m)}{\Gamma(\alpha)\alpha^m} \sum_{\substack{i,j,k,l,\ldots \in \{1,\ldots,2m\} \\ i\neq j\neq k\neq l\neq \ldots \\ \textit{all permutations}}} C_{ij}\cdots C_{kl} \tag{C1a}$$

$$E(x_1 x_2 \cdots x_{2m+1}) = 0 \tag{C1b}$$

where C_{ij} is the covariance of x_i and x_j, and $x_1, x_2, \ldots,$ and x_{2m+1} are the coordinate components of the resultant vector $\overline{X}$. All the intensity moments can be obtained by using Equation (C1); but because the K-distribution (11) is symmetric with respect to origin, all the odd order moments (C1b) vanish accordingly.

Appendix D: PDF of Normalized K-Distributed n-Dimensional Vector

In this appendix, assuming the terrain clutter to be zero-mean K-distributed, the probability density function of its normalized data is derived. Instead of focusing on six-dimensional polarimetric data, the n-dimensional case is studied.

Consider an n-dimensional feature vector $\overline{X}$ with zero-mean K-distribution (11), choose the norm $E = \sqrt{\sum x_i^2}$ as the normalization function, and make a transformation similar to the spherical transformation in three-dimensional space

$$x_i = E r_i(\Omega); \qquad i = 1, \ldots n \tag{D1}$$

where Ω is the directional angle and is a function of relative magnitudes only.

Then in general, the Jacobian of the above transformation can be written in this form

$$J = E^{n-1} S(\Omega) \tag{D2}$$

The marginal PDF of Ω is

$$\begin{aligned} P(\Omega) &= \int_0^\infty P(\overline{X}) E^{n-1} S(\Omega) dE \\ &= \int_0^\infty \frac{1}{(2\pi)^{n/2} |\overline{\overline{C}}|^{1/2}} \frac{(2\alpha)^{n/4+\alpha/2} [E^2 f(\Omega)]^{\alpha/2-n/4}}{2^{\alpha-1}\Gamma(\alpha)} \\ &\quad \times K_{n/2-\alpha}\left[\sqrt{2\alpha}(E^2 f(\Omega))^{1/2}\right] E^{n-1} S(\Omega) dE \end{aligned} \tag{D3}$$

where

$$f(\Omega) = \frac{\overline{X}^T \cdot \overline{\overline{C}}^{-1} \cdot \overline{X}}{E^2} \tag{D4}$$

After the integration is carried out, the marginal PDF $P(\Omega)$ is given as

$$P(\Omega) = \frac{S(\Omega)\Gamma(\frac{n}{2})}{2\sqrt{\pi^n \left|\overline{\overline{C}}\right|}} \left(\frac{\overline{X}^T \cdot \overline{\overline{C}}^{-1} \cdot \overline{X}}{E^2} \right)^{-n/2} \tag{D5}$$

Assuming the *a priori* probability of a certain class is P_a, we can use $-\ln(P_a P)$ as the distance measure for a Bayesian classification scheme [23]. After substituting (D5) into this expression, we note that one of the terms will be proportional to $\ln E$. Since this term remains the same when we compute the distance measure to all classes, we can exclude this term from the definition of the distance measure. Therefore, the distance measure of the optimal Bayes classifier using normalized data can be defined as

$$D = -\ln P_a + \frac{1}{2}\ln\left|\overline{\overline{C}}\right| + \frac{n}{2}\ln \overline{X}^T \cdot \overline{\overline{C}}^{-1} \cdot \overline{X} \tag{D6}$$

Polarimetric backscatter data has dimension six, and all the components are zero mean and, in general, correlated with covariance matrix, $\overline{\overline{C}} = E\left\{\overline{X}\overline{X}^T\right\}$.

Acknowledgments

This work was supported by NASA Contract NAGW-1617, NASA Contract 958461, ARMY Corp of Engineers Contract DACA39-87-K-0022, and the European Space Agency.

This work was also sponsored by the U. S. Air Force under Contract F19628-C-85-0002. The views expressed are those of the authors and do not reflect the official policy or position of the U.S. Government.

References

[1] Kong, J. A., A. A. Swartz, H. A. Yueh, L. M. Novak, and R. T. Shin, "Identification of terrain cover using the optimum polarimetric classifier," *J. Electro. Waves Applic.*, **2(2)** 171–194, 1988.

[2] Yueh, H. A., A. A. Swartz, J. A. Kong, R. T. Shin, and L. M. Novak, "Bayes classification of terrain cover using normalized polarimetric data," *J. Geophys. Res.*, **93(B12)** 15261–15267, Dec. 1988.

[3] Lim, H., A. A. Swartz, H. A. Yueh, J. A. Kong, R. T. Shin, and J. J. van Zyl, "Classification of earth terrain using synthetic aperture radar images," *J. Geophys. Res.*, **93(B12)**, 15252–15260, 1989.

[4] Evans, D. L., T. G. Farr, J. P. Ford, T. W. Thompson, and C. L. Werner, "Multipolarization radar images for geologic mapping and vegetation discrimination," *IEEE Trans. Geosci. Remote Sensing,* **GE-24(2)**, 246–256, 1986.

[5] Wu, S. T., and S. A. Sader, "Multipolarization SAR data for surface feature delineation and forest vegetation characterization," *IEEE Trans. Geosci. Remote Sensing,* **GE-25(1)**, 67–76, 1987.

[6] Zebker, H. A., J. J. van Zyl, and D. N. Held, "Imaging radar polarimetry from wave synthesis," *J. Geophys. Res.*, **92(B1)**, 683–701, 1987.

[7] van Zyl, J. J., H. A. Zebker, and C. Elachi, "Imaging radar polarization signature: theory and observation," *Radio Science,* **22(4)**, 529–543, 1987.

[8] Blom, R. G., L. R. Schenck, and R. E. Alley, "What are the best radar wavelengths, incidence angles, and polarizations for discrimination among lava flows and sedimentary rocks? A statistical approach," *IEEE Trans. Geosci. Remote Sensing,* **GE-25(2)**, 208–213, 1987.

[9] Trunk, G. V., "Non-Rayleigh sea-clutter: Properties and detection of targets," *Automatic Detection and Radar Data Processing,* D. C. Schleher Ed., Artech House, 1980.

[10] Jao, J. K., "Amplitude distribution of composite terrain radar clutter and the K-distribution," *IEEE Trans. Antennas Propagat.* **AP-32(10)**, 1049–1062, 1984.

[11] Jakeman, E. and P. N. Pusey, "A model for non-Rayleigh sea echo," *IEEE Trans. Antennas Propagat.* **AP-24(6)**, 806–814, 1976.

[12] McWhiter, J. G., and P. N. Pusey, "Enhanced fluctuations in radiation scattered by a random phase screen," *J. Opt. Soc. Am.,*

66(11), 1175–1182, 1976.

[13] Jakeman, E., "On the statistics of K-distributed noise," *J. Phys. A: Math. Gen.*, **13**, 31–48, 1980.

[14] Schätzel, K., "K-distributed phase differences in turbulent random phase screens," *J. Opt. Soc. Am.*, **73(3)**, 269–276, 1983.

[15] Barakat, R., "Weak-scatterer generalization of the K-density function with application to laser scattering in atmospheric turbulence," *J. Opt. Soc. Am. A*, **3(4)**, 401–409, 1986.

[16] Barakat, R., "Weak-scatterer generalization of the K-density function. II. Probability density of total phase," *J. Opt. Soc. Am. A*, **4(7)**, 1213–1219, 1987.

[17] Jakeman, E., and R. J. A. Tough, "Generalized K distribution: a statistical model for weak scattering," *J. Opt. Soc. Am. A*, **4(9)**, 1764–1772, 1987.

[18] Andrews, L. C., and R. L. Phillips, "I-K distribution as a universal propagation model of laser beams in atmospheric turbulence," *J. Opt. Soc. Am. A*, **2(2)**, 160–163, 1985.

[19] Shin, R. T., L. M. Novak, and M. Borgeaud, "Theoretical models for polarimetric radar clutter," Tenth DARPA/Tri-Service Millimeter Wave Symposium, U.S. Army Harry Diamond Laboratories, Adelphi, MD, April 8-10, 1986.

[20] Borgeaud, M., R. T. Shin, and J. A. Kong, "Theoretical models for polarimetric radar clutter," *J. Electro Waves Applicat.*, **1(1)**, 67–86, 1987.

[21] Yueh, S. H., J. A. Kong, J. K. Jao, R. T. Shin, and L. M. Novak, "K-distribution and polarimetric terrain radar clutter," *J. Electro. Waves Applicat.*, **3(8)**, 747–768, 1989.

[22] Novak, L. M., M. B. Sechtin, and M. J. Cardullo, "Studies on target detection algorithms which use polarimetric radar data," *IEEE Trans. Aerospace and Electronic Systems*, **AES-25(2)**, 1989.

[23] Fukunaga, K., *Introduction to Statistical Pattern Recognition*, Academic Press, New York, 1972.

[24] Durden, S. L., J. J. van Zyl, and H. A. Zebker, "The unpolarized component in polarimetric radar observations of forested areas," *IEEE Trans. Geosci. Remote Sensing*, **28(2)**, 268-271, 1990.

[25] Horn, R., "C-band SAR results obtained by an experimental airborne SAR sensor," *Proc. IGARSS,* Vancouver, Canada, July 10-14, 2213–2216, 1989.

[26] Moreira, J., "A new method of aircraft motion error extraction from radar raw data for real time SAR motion compensation," *Proc. IGARSS,* Vancouver, Canada, July 10-14, 2217–2220, 1989.